

Hidden sector monopole, vector dark matter and dark radiation with Higgs portal

Seungwon Baek, P. Ko and Wan-II Park

School of Physics, KIAS,
Seoul 130-722, Korea

E-mail: sbaek1560@gmail.com, sko@kias.re.kr, wipark@kias.re.kr

Abstract. We show that the 't Hooft-Polyakov monopole model in the hidden sector with Higgs portal interaction makes a viable dark matter model, where monopole and massive vector dark matter (VDM) are stable due to topological conservation and the unbroken subgroup $U(1)_X$. We show that, even though observed CMB data requires the dark gauge coupling to be quite small, a right amount of VDM thermal relic can be obtained via s -channel resonant annihilation for the mass of VDM close to or smaller than the half of SM higgs mass, thanks to Higgs portal interaction. Monopole relic density turns out to be several orders of magnitude smaller than observed dark matter relic density. Direct detection experiments, particularly, the projected XENON1T experiment, may probe the parameter space where the dark Higgs is lighter than $\lesssim 60$ GeV. In addition, the dark photon associated with unbroken $U(1)_X$ contributes to the radiation energy density at present, giving $\Delta N_{\text{eff}}^{\nu} \sim 0.1$ as the extra relativistic neutrino species.

Contents

1	Introduction	1
2	Model and Particle Spectra	2
3	Low energy phenomenology	3
3.1	Vacuum Stability and Perturbative Unitarity	3
3.2	Phenomenology of Two Scalar Bosons	4
4	Dark matter phenomenology	4
4.1	Self interaction between dark matters	5
4.2	Constraint from CMB	6
4.3	Relic Densities of monopoles and VDMs	10
4.3.1	VDMs	10
4.3.2	Monopoles	11
4.4	Direct Detection	12
4.4.1	VDMs	12
4.4.2	Monopoles	13
5	Dark Radiation	14
6	Conclusions	15

1 Introduction

One of the mysteries of the universe is that 26 % of it is made of nonbaryonic cold dark matter (CDM) [1], which definitely calls for beyond the SM (BSM) physics. As of now, very little is known about the particle nature of CDM except that it carries no electric or color charge. We do not know (i) how many species of CDM's are there, (ii) if DM is absolutely stable or have very long lifetime, (iii) what are the masses and spins of CDM's, and (iv) how CDMs interact with each other or the ordinary matter. This lack of information results in many models for dark matter. Very often some ad hoc Z_2 symmetry or similar is introduced in order to stabilize DM without questioning the origin of those symmetries. Also, DM particles often feel no gauge interaction, unlike most of the SM particles. However weakly interacting massive particle (WIMP) with mass $\sim O(100)$ GeV, which is the most common CDM candidate, is not likely to be stable under a global symmetry which is often assumed for the stability of DM [2]. The stability of DM and the fact that SM is guided by local gauge principle may imply that the dark sector in which the dark matter responsible for the present relic density resides may respect local gauge symmetry, too. This picture also arises naturally in string inspired models [3].

The last unbroken dark gauge symmetry (H_X) guaranteeing the stability of DM may be originated from a larger gauge group (G_X). In this case, topologically stable objects are likely to form during the symmetry-breaking phase transition, although it depends on the nature of the larger gauge group and the pattern of the symmetry breaking. For example one can have topological monopole if $\Pi_2(G_X/H_X) = Z$ (integer), vortices (strings) or domain

walls depending on the lower homotopy classes. Moreover, since the hidden sector may communicate with the visible sector via various gauge singlet portal interactions [2], even topological soliton(s) may have a chance to leave observable imprints.

In this paper, we consider a simple hidden sector DM model, where non-Abelian dark gauge symmetry $SU(2)_X$ is broken down to a $U(1)_X$ by a real triplet dark Higgs field. It is just the 't Hooft-Polyakov monopole [4, 5] model in the hidden sector. In this well known setup, we add the Higgs portal interaction which is allowed at renormalizable level, and show that a viable dark matter phenomenology can be obtained.

This paper is organized as follows. In section 2, our model is proposed and particle spectra in the model is discussed. In section 3, we discuss about constraints coming from the vacuum stability, perturbative unitarity and collider data. Section 4 is devoted to DM-phenomenology, where constraints on DM self-interaction from formation of massive black holes and CMB data are discussed, and relic densities of VDM and monopoles are estimated. In section 5, dark radiation is discussed briefly, and conclusion is drawn in section 6.

2 Model and Particle Spectra

Let us consider $SU(2)_X$ -triplet real scalar field $\vec{\Phi}$ with the following Lagrangian:

$$\mathcal{L} = \mathcal{L}_{\text{SM}} - \frac{1}{4} V_{\mu\nu}^a V^{a\mu\nu} + \frac{1}{2} D_\mu \vec{\Phi} \cdot D^\mu \vec{\Phi} - \frac{\lambda_\Phi}{4} \left(\vec{\Phi} \cdot \vec{\Phi} - v_\Phi^2 \right)^2 - \frac{\lambda_{\Phi H}}{2} \left(\vec{\Phi} \cdot \vec{\Phi} - v_\Phi^2 \right) \left(H^\dagger H - \frac{v_H^2}{2} \right) \quad (2.1)$$

where \mathcal{L}_{SM} is the standard model Lagrangian, $D_\mu \Phi^a = \partial_\mu \Phi^a - g_X \epsilon^{abc} V_\mu^b \Phi^c$ and $V_{\mu\nu}^a = \partial_\mu V_\nu^a - \partial_\nu V_\mu^a - g_X \epsilon^{abc} V_\mu^b V_\nu^c$ with ϵ^{abc} ($a, b, c = 1, 2, 3$) being the structure constant of the hidden sector $SU(2)$ gauge group. The Higgs portal interaction is described by the $\lambda_{\Phi H}$ term. When we ignore the Higgs portal interaction, the hidden sector Lagrangian describes the 't Hooft-Polyakov monopole [4, 5]. After the spontaneous symmetry breaking of $SU(2)_X \approx SO(3)_X$ into $U(1)_X \approx SO(2)_X$ by nonzero vacuum expectation value (VEV) of $\vec{\Phi}$,

$$\langle \vec{\Phi}(x) \rangle = (0, 0, v_\Phi),$$

hidden sector particles are composed of massive dark vector bosons $V_\mu^\pm \equiv (V_\mu^1 \mp iV_\mu^2)/\sqrt{2}$ with masses $m_V = g_X v_\Phi$ ¹, massless dark photon $\gamma_{h,\mu} \equiv V_\mu^3$, massive real scalar ϕ (dark Higgs boson) and topologically stable heavy (anti-)monopole with mass $m_M = m_V/\alpha_X$.

After the spontaneous breaking of electroweak symmetry, Higgs portal interaction mixes ϕ and SM Higgs boson h . After imposing the vanishing tadpole conditions, the mass² mixing between h and ϕ is described by the following matrix:

$$\begin{pmatrix} m_{hh}^2 & m_{\phi h}^2 \\ m_{\phi h}^2 & m_{\phi\phi}^2 \end{pmatrix} \equiv \begin{pmatrix} 2\lambda_H v_H^2 & \lambda_{\phi H} v_H v_\phi \\ \lambda_{\phi H} v_H v_\phi & 2\lambda_\phi v_\phi^2 \end{pmatrix} \quad (2.2)$$

in the (h, ϕ) basis with λ_H being the quartic coupling of the SM Higgs. We can make a $SO(2)$ rotation from (h, ϕ) basis to the physical mass eigenstates, (H_1, H_2) with mass eigenvalues

$$m_{1,2}^2 = \frac{1}{2} \left[(m_{hh}^2 + m_{\phi\phi}^2) \mp \sqrt{(m_{hh}^2 - m_{\phi\phi}^2)^2 + 4m_{\phi h}^4} \right] \quad (2.3)$$

¹Here ± 1 indicate the dark charge under $U(1)_X$, and not ordinary electric charges.

Note that $m_{1,2}^2 > 0$ requires $\lambda_{\phi H} < 2\sqrt{\lambda_H \lambda_\phi}$. With the mixing angle α defined by

$$\tan 2\alpha = \frac{2m_{\phi H}^2}{m_{hh}^2 - m_{\phi\phi}^2} \quad (2.4)$$

the interaction eigenstates can be expressed in terms of mass eigenstates as

$$\begin{pmatrix} h \\ \phi \end{pmatrix} = \begin{pmatrix} \cos \alpha & -\sin \alpha \\ \sin \alpha & \cos \alpha \end{pmatrix} \begin{pmatrix} H_1 \\ H_2 \end{pmatrix} \quad (2.5)$$

This is similar to the renormalizable models for singlet fermion DM [6, 7] or VDM [8].

Note that there is no kinetic mixing between γ_h and the SM $U(1)_Y$ -gauge boson unlike the $U(1)_X$ -only case, due to the non Abelian nature of the hidden gauge symmetry. The hidden vector bosons V_μ^\pm are absolutely stable due to the unbroken $U(1)_X$ gauge symmetry even if we consider nonrenormalizable interactions. Hence they become good CDMs in addition to monopoles without additional dark charged matter fields. This aspect is in sharp contrast with the VDM with the $SU(2)_X$ being completely broken [9], where the stability of massive VDM is not protected by $SU(2)_X$ gauge symmetry and nonrenormalizable interactions would make the VDM decay in general. In the model presented in this paper, the unbroken $U(1)_X$ subgroup not only protects the stability of VDM V_μ^\pm , but also contributes to the dark radiation at the level of ~ 0.1 .

3 Low energy phenomenology

The presence of symmetry breaking *dark higgs* field and *Higgs portal* interaction allows a mixing between SM- and dark-Higgs bosons. This mixing improves the vacuum stability of SM Higgs potential, but is constrained by collider experiments as described below.

3.1 Vacuum Stability and Perturbative Unitarity

The Higgs portal interaction of Φ to the SM Higgs H can improve the vacuum stability along SM Higgs direction up to Planck scale via tree-level $h - \phi$ mixing and additional scalar loop-correction to the quartic coupling of SM Higgs. As shown in Ref. [7], for $m_t = 173.2$ GeV and $\alpha_s = 0.118$ as the top-quark pole mass and strong gauge coupling, the vacuum instability can be cured up to Planck scale, if $m_1 < m_2$ and the scalar mixing angle (α) satisfies

$$\lambda_H = \lambda_H^{\text{SM}} \left[1 - \left(1 - \frac{m_2^2}{m_1^2} \right) \sin^2(\alpha) \right] \gtrsim 0.139, \quad (3.1)$$

where $\lambda_H^{\text{SM}} \equiv m_h^2 / (2v_H^2) \simeq 0.129$ is the Higgs quartic coupling of SM with $m_1 = m_h \approx 125$ GeV being the mass of the observed SM high-like particle, or $0.2 \lesssim \lambda_{\phi H} \lesssim 0.6$ with $0 \leq \lambda_\phi \lesssim 0.2$.

Recent result from LHC experiments constrains the mixing angle to be $\alpha \lesssim 0.45$ at 95% CL [11]. For such a small mixing, the mass eigenstates can be approximated to the interaction eigenstates, and in case of absolute stability Eq. (3.1) is translated to $m_\phi \gtrsim 150$ GeV if $\lambda_{\phi H}$ is too small to improve the vacuum stability. Note that, if $m_2 < m_1$, vacuum instability becomes worse for a non-zero α , and hence somewhat large $\lambda_{\phi H}$ would be necessary. However, for a small α satisfying $\tan \alpha \lesssim m_\phi / m_h$, tachyon-free condition $\lambda_{\phi H} < 2\sqrt{\lambda_\phi \lambda_H}$ is translated to

$$\lambda_{\phi H} \lesssim \sqrt{\frac{g_X m_\phi}{m_V} \left[1 - \left(1 - \frac{m_\phi^2}{m_h^2} \right) \sin^2 \alpha \right] \frac{m_h^2}{v_H^2}} \quad (3.2)$$

implying that the small m_V is, the larger $\lambda_{\Phi H}$ can be. In addition, as will be discussed in section 4.2 and 4.3, in order to be consistent with CMB constraint and to obtain a right amount of relic density, one needs

$$2m_V \approx m_\phi \text{ or } m_h \quad (3.3)$$

Moreover, for such a light VDM, g_X is constrained by small scale structure as Eq. (4.4). Hence, for $m_\phi < m_h$ and $2m_V \approx m_\phi$, Eq. (3.2) can be written as

$$\lambda_{\Phi H} \lesssim 7.6 \times 10^{-2} \left(\frac{m_V}{50 \text{ GeV}} \right)^{3/8} \left[1 - \left(1 - \frac{4m_V^2}{m_h^2} \right) \sin^2 \alpha \right]^{1/2} \quad (3.4)$$

which looks a bit small to cure vacuum instability problem. Therefore, in case of $m_\phi < m_h$, SM vacuum might be meta-stable modulo uncertainties in the pole mass of top quark and the strong coupling constant α_s .

3.2 Phenomenology of Two Scalar Bosons

For $m_\phi > 2m_h$, the decay channel of 4-charged-lepton final states is open (see [8] for details) and provide a clean signal. It might be within the reach of LHC experiments. On the other hand, if $m_\phi < m_h/2$, SM higgs can decay into two lighter dark Higgs bosons which decay subsequently to light SM particles. Since λ_ϕ and $\lambda_{\phi H}$ is much smaller than λ_H in this case (see the next section), the decay of SM Higgs to dark Higgs is mainly due to λ_H coupling, and the decay rate is found to be

$$\Gamma_{h \rightarrow \phi\phi} = \frac{9 (c_\alpha s_\alpha^2)^2 m_h^3}{32\pi v_H^2} \left(1 - \frac{4m_\phi^2}{m_h^2} \right)^{1/2} \quad (3.5)$$

where $m_h \simeq \sqrt{2\lambda_H} v_H$ was used. The subsequent decay rate of ϕ would be the same as that of SM-like Higgs boson, with the replacement $m_h \leftrightarrow m_\phi$ and a universal suppression factor $\sin^2 \alpha$ in the decay rate for each channel. Therefore, the decay of SM-like Higgs to dark Higgs bosons will produce dominantly 4 b-jets, if kinematically allowed ($m_\phi > 2m_b \sim 10 \text{ GeV}$). LEP Higgs search imposes a bound on such a process and requires $\alpha \lesssim 0.3$ for $m_\phi \lesssim 60 \text{ GeV}$, as shown in Fig. 1. LHC experiments also impose a bound on the branching fraction of the SM-like Higgs boson into non-SM channels, as shown in Fig. 2 where we used an approximation [11]

$$c_\alpha \geq 0.904 + \text{Br}_{\text{non-SM}}/2$$

with $\text{Br}_{\text{non-SM}}$ being the branching fraction of the decay of SM-like higgs to non-SM channels.

Note that for nonzero scalar mixing angle ($\alpha \neq 0$), the signal strength of the SM Higgs-like scalar boson is less than 1 in a universal manner [2, 6, 8], which is a generic in Higgs portal DM models with only one Higgs doublet as in the SM.

4 Dark matter phenomenology

The massless dark photon (γ_h) in our scenario mediates a long range force between vector dark matters (V_μ^\pm) and (anti)monopoles. Particularly, such a massless mediator can cause a

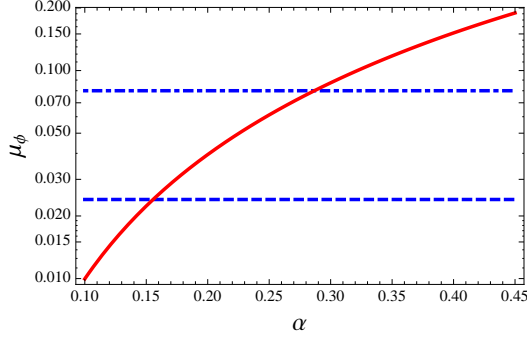


Figure 1. Signal strength (solid red line) of SM channels caused by the production and decay of dark higgs, as a function of α . Blue dashed and dot-dashed lines are the upper-bound at 95% CL for $m_\phi \approx 20, 60$ GeV, respectively [10].

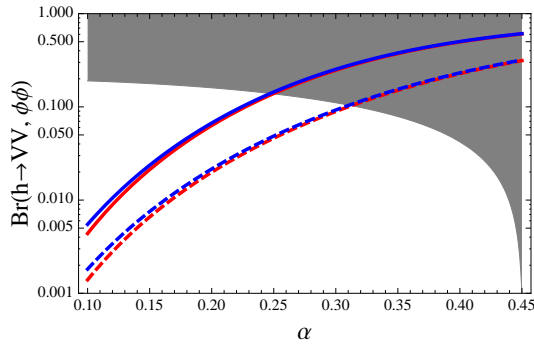


Figure 2. Branching fraction of the decay of SM-like Higgs to non-SM (two VDMs or dark higgs), as a function of α . Red: $m_V = (1 - 3/40) \times m_h/2$, Blue: $m_V = (1 - 3/40) \times m_\phi/2$. To be consistent with the constraint described in the next section, $g_X = 4.5 \times 10^{-2} (2m_V/1 \text{ TeV})^{3/4}$ was used. Solid and dashed lines correspond to $m_\phi = 20, 60$ GeV, respectively. Gray region is excluded by collider experiments at 95% CL [11].

large non-perturbative enhancement of perturbative pair annihilation or self-interactions of dark matter. The enhancement, named as Sommerfeld enhancement, is given by [12, 13]

$$\mathcal{S} = \frac{\pi\alpha_X/v}{1 - e^{-\pi\alpha_X/v}} \quad (4.1)$$

where v is the velocity of dark matter. Note that, when $v \ll \alpha_X$, the enhancement is proportional to $1/v$. This behavior of \mathcal{S} has crucial impacts on CMB and physics of small scale dark matter subhalos, as described in the following two subsections. For simplicity, we begin with the constraint from small scale dark matter subhalos.

4.1 Self interaction between dark matters

The dark photon carries a long range dark force between monopoles and VDMs. For the main component of dark matter, the self-interaction is strongly constrained by small and large scale structures (dwarf galaxies, bullet cluster, etc.), similarly to the singlet portal scalar DM considered in Ref.s [2, 14]. Since monopole contribution to dark matter of the universe turns out to be subdominant as described in the section 4.3, we will consider only the case of VDM self-interactions in this subsection.

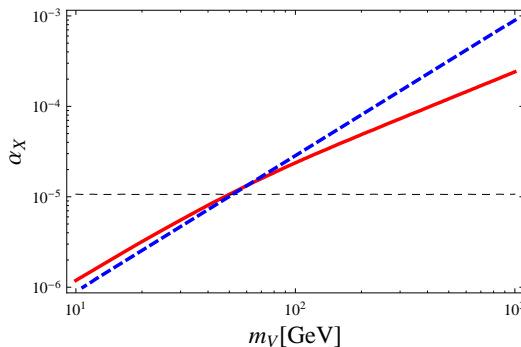


Figure 3. Bound on α_X (red line) obtained from Eq. (4.3) as a function of m_V . Dashed blue line is the case when enhancement factor is ignored. Horizontal dashed black line corresponds to $\pi\alpha_X/v_{\text{cm}} = 1$ with $v_{\text{cm}} = 10\text{km/sec}$ being the velocity of dark matter at subhalos of dwarf galaxy scale.

The transfer cross section of the VDM self-interaction mediated by dark photon is

$$\sigma_T = \mathcal{S} \times \frac{\pi\alpha_X^2}{m_V^2 v_{\text{cm}}^4} \ln \left[\frac{m_V^2 v_{\text{cm}}^3}{(4\pi\rho_V\alpha_X^3)^{1/2}} \right] \quad (4.2)$$

where v_{cm} and ρ_V are respectively the velocity and energy density of dark matter at the region of interest, and only the contribution from attractive interaction was included since repulsive interaction causes suppression rather than enhancement. Formation of massive blackholes caused by DM self-interaction [15] may impose the most strong bound [16]:

$$\frac{\sigma_T}{m_V} \lesssim \left(\frac{\sigma_T}{m_V} \right)^{\text{max}} \equiv 35\text{cm}^2/\text{g} \text{ for } v_{\text{cm}} = 10\text{km/s} \quad (4.3)$$

leading to an upper-bound on α_X that is depicted in Fig. 3 as a function of m_V . For $\alpha_X \lesssim v/\pi$ leading to $\mathcal{S} \sim 1$, the constraint can be interpreted approximately as

$$\alpha_X \lesssim 10^{-5} \left(\frac{m_V}{50\text{GeV}} \right)^{3/2} \quad (4.4)$$

where $v_{\text{cm}} = 10\text{km/s}$ and $\rho_V = 3\text{GeV}/\text{cm}^3$ were used. In fact, Eq. (4.4) is valid for $10\text{GeV} \lesssim m_V \lesssim 100\text{GeV}$, which will be the range of our prime interest, within $\mathcal{O}(10)\%$ error.

Interestingly, for $\alpha_X^{\text{max}}/10^2 \lesssim \alpha_X \lesssim \alpha_X^{\text{max}}$ with α_X^{max} being the upper-bound of α_X , self-interactions among VDM can resolve the core/cusp problem and “too-big-to-fail” problem of the conventional collisionless CDM scenarios [16, 17].

4.2 Constraint from CMB

Around the epoch of CMB decoupling, the velocity of dark matter is given by

$$v_{\text{cmb}} = v' \left[\frac{g_{*S}(T_{\text{cmb}})}{g_{*S}(T')} \right]^{1/3} \frac{T_{\text{cmb}}}{T'} \quad (4.5)$$

where v is the velocity of dark matter, T is the photon temperature, and ‘ \prime ’ and the subscript ‘ $_{\text{cmb}}$ ’ denote the epochs of DM’s last kinetic decoupling and CMB decoupling, respectively. If DM is kinetically decoupled from visible sector at $T = T_{\text{kd}}$ while it is still coupled to dark

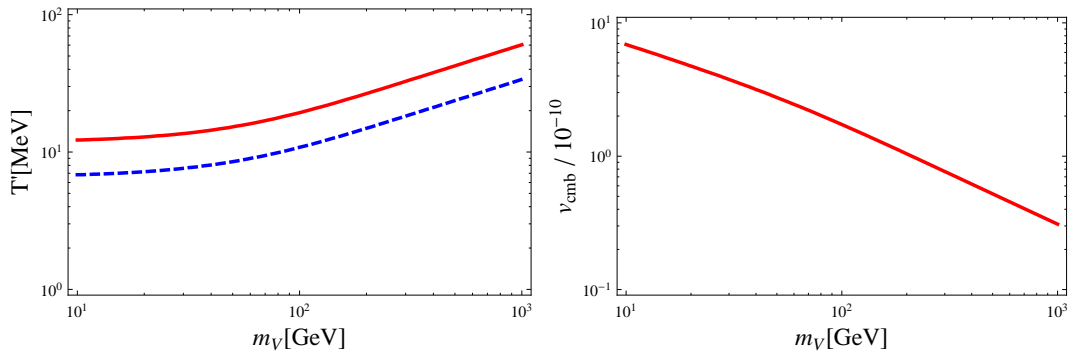


Figure 4. Left: Temperatures of photon (T' : red solid line) and dark photon ($T'_{\gamma'}$: blue dashed line) at the last kinetic decoupling of dark matter. Right: Velocity of dark matter around the epoch of CMB decoupling (v_{cmb}). We used α_X saturating the bound from small scale structures.

photon, the thermal bath around the epoch of the last kinetic decoupling is provided by dark photon. In this case, the temperature of dark photon $T_{\gamma'}$ for $T < T_{\text{kd}}$ is given by

$$T_{\gamma'} = \left(\frac{g_{*S}(T)}{g_{*S}(T_{\text{kd}})} \right)^{1/3} T \quad (4.6)$$

The Compton scattering rate of DM to dark photon when the temperature of dark photon is $T_{\gamma'}$ is

$$\Gamma_{\text{Comp}} = \frac{32\pi^3 \alpha_X^2 T^4}{45m_V^3} \left(\frac{g_{*S}(T)}{g_{*S}(T_{\text{kd}})} \right)^{4/3} \quad (4.7)$$

Comparing to the expansion rate, $H = (\pi^2 g_*(T)/90)^{1/2} T^2/M_{\text{P}}$, one finds that the photon temperature when DM is kinetically decoupled from dark photon is

$$T' = \left(\frac{45}{32\pi^3 \alpha_X^2} \right)^{1/2} \left(\frac{g_{*S}(T')}{g_{*S}(T_{\text{kd}})} \right)^{-2/3} \left(\frac{\pi^2}{90} g_*(T') \right)^{1/4} \left(\frac{m_V}{M_{\text{P}}} \right)^{3/2} M_{\text{P}} \quad (4.8)$$

Hence, using $v' = \sqrt{3T'_{\gamma'}/m_V}$ and Eq. (4.6), one finds

$$v_{\text{cmb}} = \left(\frac{32\pi^3 \alpha_X^2}{5} \right)^{1/4} \left(\frac{3\sqrt{10}}{\pi} \right)^{1/4} \frac{g_{*S}(T')^{1/24} g_{*S}(T_{\text{cmb}})^{1/3}}{g_{*S}(T_{\text{kd}})^{1/2}} \left(\frac{T_{\text{cmb}}}{M_{\text{P}}} \right) \left(\frac{M_{\text{P}}}{m_V} \right)^{5/4} \quad (4.9)$$

where we used $g_*(T') = g_{*S}(T')$. Fig. 4 shows temperatures of photon and dark photon (left panel), and v_{cmb} (right panel) at the last kinetic decoupling as functions of m_V .

The present CMB data constrains the velocity-averaged annihilation cross section of dark matter to SM particles to be upper-bounded at [18]

$$\begin{aligned} \langle \sigma v_{\text{rel}} \rangle_{\text{tot}}^{\text{cmb}} &= \frac{0.66 \times 10^{-6} m_V}{\sum_{i=\text{channels}} f_{\text{eff,sys}}^i \text{Br}^i} \left(\frac{\text{m}^3}{\text{sec} \cdot \text{kg}} \right) \\ &\simeq \frac{1.2 \times 10^{-24}}{\sum_{i=\text{channels}} f_{\text{eff,sys}}^i \text{Br}^i} \left(\frac{m_V}{1 \text{ TeV}} \right) \text{cm}^3/\text{sec} \end{aligned} \quad (4.10)$$

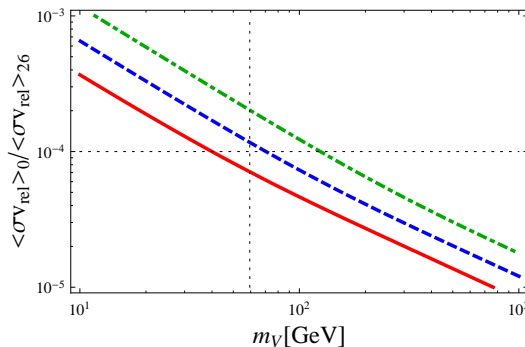


Figure 5. Upper bound of $\langle \sigma v_{\text{rel}} \rangle_0 / \langle \sigma v_{\text{rel}} \rangle_{26}$ around the epoch of CMB decoupling. Solid red, dashed blue and dot-dashed green correspond to α_X saturating the upper-bound $a \times (\sigma_T / m_V)^{\text{max}}$ with $a = 1, 10^{-1}, 10^{-2}$, respectively. We used $\sum_{i=\text{channels}} f_{\text{eff,sys}}^i \text{Br}^i = 0.1$.

where $f_{\text{eff,sys}}^i$ and Br^i are respectively the fractional energy deposition of annihilation products and the branching fraction of channel i . The total annihilation cross section can be expressed as

$$\langle \sigma v_{\text{rel}} \rangle_{\text{tot}} = \langle \sigma v_{\text{rel}} \rangle_0 \mathcal{S} \quad (4.11)$$

where $\langle \sigma v_{\text{rel}} \rangle_0$ is the perturbative annihilation cross section. Then, requiring $\langle \sigma v_{\text{rel}} \rangle_{\text{tot}} < \langle \sigma v_{\text{rel}} \rangle_{\text{tot}}^{\text{cmb}}$, we find

$$\begin{aligned} \frac{\langle \sigma v_{\text{rel}} \rangle_0}{\langle \sigma v_{\text{rel}} \rangle_{26}} &< \frac{20/\mathcal{S}}{\sum_{i=\text{channels}} f_{\text{eff,sys}}^i \text{Br}^i} \left(\frac{m_V}{1 \text{ TeV}} \right) \\ &\simeq \frac{(20/\pi) \times 10^{-6}}{\sum_{i=\text{channels}} f_{\text{eff,sys}}^i \text{Br}^i} \left(\frac{v_{\text{cmb}}}{10^{-10}} \right) \left(\frac{10^{-5}}{\alpha_X} \right) \left(\frac{m_V}{100 \text{ GeV}} \right) \end{aligned} \quad (4.12)$$

where $\langle \sigma v_{\text{rel}} \rangle_{26} \equiv 6 \times 10^{-26} \text{ cm}^3/\text{sec}$, and we used $\mathcal{S} \approx \pi \alpha_X / v_{\text{cmb}}$ in the second line. Fig. 5 shows that $\langle \sigma v_{\text{rel}} \rangle_0$ around the epoch of CMB decoupling should be smaller than $\langle \sigma v_{\text{rel}} \rangle_{26}$ by several orders of magnitude.

A pair of V^+V^- can annihilate via the s -channel ϕ exchanges and its mixing with the SM Higgs boson h , and t -channel V^\pm exchanges. Hence the total annihilation cross section without nonperturbative enhancement effect taken into account is given by

$$\begin{aligned} (\sigma v_{\text{rel}})_0 &= (\sigma v_{\text{rel}})_{VV \rightarrow \text{SM}}^s + (\sigma v_{\text{rel}})_{VV \rightarrow \gamma_h \gamma_h}^t \\ &\quad + (\sigma v_{\text{rel}})_{VV \rightarrow H_1 H_1}^t + (\sigma v_{\text{rel}})_{VV \rightarrow H_2 H_2}^t + (\sigma v_{\text{rel}})_{VV \rightarrow H_1 H_2}^t \end{aligned} \quad (4.13)$$

where

$$\begin{aligned}
(\sigma v_{\text{rel}})_{VV \rightarrow \text{SM}}^s &= \frac{1}{2s} m_V^2 \alpha_X \sin^2(2\alpha) \left| \sum_{i=1,2} \frac{(-1)^{i+1}}{s - m_i^2 + i\Gamma_i m_i} \right|^2 \left[12 - 4 \left(\frac{s}{m_V^2} \right) + \left(\frac{s}{m_V^2} \right)^2 \right] \\
&\quad \left\{ \frac{1}{144} \left(1 - \frac{4m_W^2}{s} \right)^{1/2} m_W^2 g^2 \left[12 - 4 \left(\frac{s}{m_W^2} \right) + \left(\frac{s}{m_W^2} \right)^2 \right] \right. \\
&\quad + \frac{1}{2 \times 144} \left(1 - \frac{4m_Z^2}{s} \right)^{1/2} m_Z^2 \left(\frac{g}{\cos \theta_W} \right)^2 \left[12 - 4 \left(\frac{s}{m_Z^2} \right) + \left(\frac{s}{m_Z^2} \right)^2 \right] \\
&\quad \left. + \frac{1}{18} \sum_f N_{c,f} \left(1 - \frac{4m_f^2}{s} \right)^{3/2} \left(\frac{m_f}{2m_W} \right)^2 g^2 s \right\} \quad (4.14)
\end{aligned}$$

$$\begin{aligned}
(\sigma v_{\text{rel}})_{VV \rightarrow H_i H_j}^s &= \frac{\mathcal{S}_{ij} \alpha_X m_V^2}{36\pi s} \left| \frac{s_\alpha \lambda_{1ij}}{s - m_1^2 + i\Gamma_1 m_1} + \frac{c_\alpha \lambda_{2ij}}{s - m_2^2 + i\Gamma_2 m_2} \right|^2 \\
&\quad \left[12 - 4 \left(\frac{s}{m_V^2} \right) + \left(\frac{s}{m_V^2} \right)^2 \right] \left[1 + \left(\frac{m_i^2 - m_j^2}{s} \right)^2 - 2 \left(\frac{m_i^2 + m_j^2}{s} \right) \right]^{1/2} \quad (4.15)
\end{aligned}$$

$$(\sigma v_{\text{rel}})_{VV \rightarrow \gamma_h \gamma_h}^t = \frac{\pi \alpha_X^2}{9m_V^2 \beta} \left[44\beta - 18\beta^3 + 6\beta^5 - 3(1 - \beta^2)^2(1 + \beta^2) \log \frac{1 + \beta}{1 - \beta} \right] \quad (4.16)$$

$$(\sigma v_{\text{rel}})_{VV \rightarrow H_1 H_1}^t = \frac{\pi}{s} \alpha_X^2 \sin^4 \alpha \left(1 - \frac{4m_1^2}{s} \right)^{1/2} \left[12 - 4 \left(\frac{s}{m_V^2} \right) + \left(\frac{s}{m_V^2} \right)^2 \right]$$

$$(\sigma v_{\text{rel}})_{VV \rightarrow H_2 H_2}^t = \frac{\pi}{s} \alpha_X^2 \cos^4 \alpha \left(1 - \frac{4m_2^2}{s} \right)^{1/2} \left[12 - 4 \left(\frac{s}{m_V^2} \right) + \left(\frac{s}{m_V^2} \right)^2 \right]$$

$$\begin{aligned}
(\sigma v_{\text{rel}})_{VV \rightarrow H_1 H_2}^t &= \frac{\pi}{2s} \alpha_X^2 \sin^2(2\alpha) \left[1 - \frac{(m_1 - m_2)^2}{s} \right]^{1/2} \left[1 - \frac{(m_1 + m_2)^2}{s} \right]^{1/2} \\
&\quad \times \left[12 - 4 \left(\frac{s}{m_V^2} \right) + \left(\frac{s}{m_V^2} \right)^2 \right] \quad (4.17)
\end{aligned}$$

with α and $N_{c,f}$ being respectively the mixing angle and the color factor of the SM fermion f , $\mathcal{S}_{ij} = (1/2, 1)$ for $(i = j, i \neq j)$,

$$\lambda_{111} = 6\lambda_\phi v_\phi s_\alpha^3 + 3\lambda_{\phi H} v_H c_\alpha s_\alpha^2 + 3\lambda_{\phi H} v_\phi c_\alpha^2 s_\alpha + 6\lambda_H v_H c_\alpha^3 \quad (4.18)$$

$$\lambda_{122} = \lambda_{\phi H} v_H c_\alpha^3 - 2(-3\lambda_H + \lambda_{\phi H}) v_H c_\alpha s_\alpha^2 - 2(-3\lambda_\phi + \lambda_{\phi H}) v_\phi c_\alpha^2 s_\alpha + \lambda_{\phi H} v_\phi s_\alpha^3 \quad (4.19)$$

$$\lambda_{211} = \lambda_{\phi H} v_\phi c_\alpha^3 - 2(-3\lambda_\phi + \lambda_{\phi H}) v_\phi c_\alpha s_\alpha^2 + 2(-3\lambda_H + \lambda_{\phi H}) v_H c_\alpha^2 s_\alpha - \lambda_{\phi H} v_H s_\alpha^3 \quad (4.20)$$

$$\lambda_{222} = 6\lambda_\phi v_\phi c_\alpha^3 - 3\lambda_{\phi H} v_H c_\alpha^2 s_\alpha + 3\lambda_{\phi H} v_\phi c_\alpha s_\alpha^2 - 6\lambda_H v_H s_\alpha^3 \quad (4.21)$$

and $\beta = (1 - 4m_V^2/s)^{1/2}$. We notice that, for $\alpha_X \lesssim \alpha_X^{\text{max}}$, the total annihilation cross section is generically much smaller than $\langle \sigma v_{\text{rel}} \rangle_{26}$. However, as shown in Fig. 6, $\langle \sigma v_{\text{rel}} \rangle_{\text{tot}}$ can reach $\langle \sigma v_{\text{rel}} \rangle_{26}$ around the s -channel resonance region. Hence, for the present relic density of VDM to be consistent with observation, the energy of VDM had to be in the resonance band at freeze-out. It turned out that for $\sqrt{s} \approx m_\phi \gtrsim 150 \text{ GeV}$ the resonance band is not narrow enough to satisfy both of CMB constraint and relic density requirement simultaneously. On

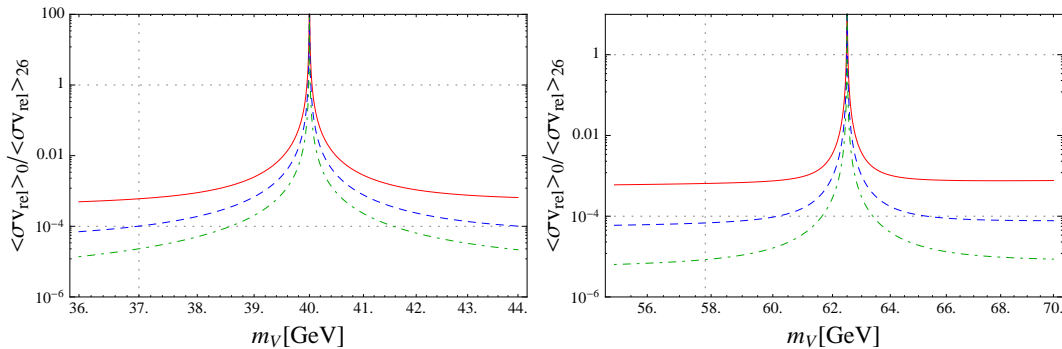


Figure 6. Velocity-averaged annihilation cross section at the CMB decoupling epoch, normalized by the canonical value for thermal relic (i.e., $\langle\sigma v_{\text{rel}}\rangle_{\text{fz}} = 6 \times 10^{-26} \text{cm}^3/\text{sec}$). Left: $m_\phi = 80 \text{ GeV}$ and $\alpha = 0.25$. Right: $m_\phi = 200 \text{ GeV}$ and $\alpha = 0.1$. Colored lines corresponds to $a = 1, 10^{-1}, 10^{-2}$ from top to bottom with a defined in Fig. 5. Dashed vertical line corresponds to $\sqrt{s}/2 - m_V \simeq (3/2)T_{\text{fz}}$ with $T_{\text{fz}} = m_V/20$ for $\sqrt{s} = m_\phi, m_h$ in the left and right panel, respectively.

the other hand, if $\sqrt{s} \approx m_\phi \lesssim 80 \text{ GeV}$ (or $\approx m_h$), and the dark gauge coupling α_X satisfies the following condition,

$$\alpha_X \lesssim \alpha_X^{\text{CMB}} \equiv \alpha_X^{\text{max}}/\sqrt{10}, \quad (4.22)$$

the resonance is quite sharp so that we can obtain a right amount of VDM relic density while satisfying the CMB constraint.

4.3 Relic Densities of monopoles and VDMs

4.3.1 VDMs

The massive vector bosons V^\pm make good CDM of the universe, and they are thermalized mainly by the Higgs portal interaction, $\lambda_{\phi H}$ term in Eq. (2.1). For $\alpha_X \lesssim \alpha_X^{\text{CMB}}$ and small mixing angle α , the annihilation cross section is typically much smaller than the canonical value for a right amount of relic density at present except for the s -channel resonance. On the s -channel resonance, for $|m_1 - m_2| \gg \text{Max}[\Gamma_1, \Gamma_2]$ with $\Gamma_{1,2}$ being the total decay width of $H_{1,2}$, the present relic density can be approximated to [27]

$$Y_{V,0}^{\text{res}} \approx C_V \frac{m_V/M_{\text{P}}}{(3/4)f_{\text{R}}(\alpha)\alpha_X} \frac{\Gamma_{\text{R}}(\alpha)}{\Gamma_{\text{R}}^{\text{SM}}(\alpha)} \frac{\Theta(\epsilon_{\text{R}})}{\text{erfc}(\sqrt{x_{\text{fz}}\epsilon_{\text{R}}})} \quad (4.23)$$

where $Y_{V,0}^{\text{res}}$ is the yield of VDM at present in the resonance band, $C_V \equiv \frac{27}{32\pi^2} \sqrt{\frac{5}{2g_*(T_{\text{fz}})}}$ with $g_*(T_{\text{fz}}) \sim 100$ being the relativistic degrees of freedom at freeze-out, m_{R} and Γ_{R} are respectively the mass and total decay width of resonance, $\Theta(x)$ is the Heaviside step-function, $\epsilon_{\text{R}} \equiv (1 - 4m_V^2/m_{\text{R}}^2) m_{\text{R}}^2/4m_V^2$, $x_{\text{fz}} \equiv m_V/T_{\text{fz}} \sim 25$, and the decay rates of a resonance to DM and SM particles are respectively given by

$$\Gamma_{\text{R}}^{\text{DM}}(\alpha) \approx f_{\text{R}}(\alpha) \frac{3}{4} \alpha_X m_{\text{R}} \epsilon_{\text{R}}^{1/2} \quad (4.24)$$

$$\Gamma_{\text{R}}^{\text{SM}}(\alpha) = (1 - f_{\text{R}}(\alpha)) \Gamma^{\text{SM}}(m_{\text{R}}) \quad (4.25)$$

where $f_{\text{R}}(\alpha) = (\sin^2 \alpha, \cos^2 \alpha)$ for $\text{R} = (1, 2)$, and $\Gamma^{\text{SM}}(m_{\text{R}})$ is the decay rate of SM Higgs in case m_h is replaced to m_{R} . As shown in the left panel of Fig. 7, defining the level of

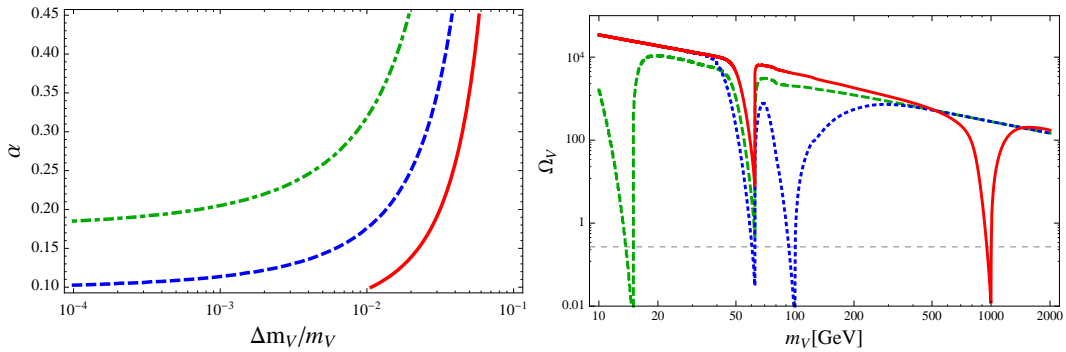


Figure 7. Left: Contours of $\Omega_{\text{VDM}} = \Omega_{\text{CDM}}^{\text{obs}}$ as a function of α and $\Delta m_V/m_V$ for $m_V \approx m_h/2 - (3/2)T_{\text{fb}}$ and $a = 1, 10^{-1}, 10^{-2}$ from right to left with a defined in Fig. 5. Right: Ω_{VDM} as a function of m_V for $m_1 = 125$ GeV and $m_2 = 30$ GeV, 0.2 TeV, 2 TeV (dashed-green, dotted-blue, solid-red). g_X was chosen to be the half of the upper-bound in Eq. (4.4), and $\alpha = 0.3m_1m_2/(m_2^2 - m_1^2)$ was used.

tuning for resonance as $\Delta m_V/m_V \equiv (\sqrt{s} - m_R)/(2m_V)$, we find that a tuning smaller than about $\mathcal{O}(1)\%$ is necessary to obtain a right amount of relic density, if $m_V \approx m_h/2$ and $\alpha_X \lesssim \alpha_X^{\text{CMB}}$. In case of $m_V \approx m_\phi$, the fine tuning parameter is approximately given by $\Delta m_V/m_V = \mathcal{O}(1 - 10)\%$ for $\alpha_X = (0.1 - 1) \times \alpha_X^{\text{max}}$. Note that it does not depend on the mixing angle α , since α -dependence is nearly cancelled out in Eq. (4.23). The right panel of Fig. 7 is the thermal relic density of hidden sector VDM, obtained by micromegas [28], as functions of m_V for $m_2 = 0.03, 0.2, 2$ TeV.

4.3.2 Monopoles

The $SU(2)$ symmetry is broken down to $U(1)_X$ as the phase transition takes place at temperature $T_c \simeq \sqrt{|m_{\phi\phi}(\phi=0)|}/\sqrt{(5/12)\lambda_\phi + g_X^2/2}$ with $m_{\phi\phi}^2(\phi=0) = -\lambda_\phi v_\phi^2$ being the zero temperature mass of ϕ at the origin. The strength of the phase transition characterized by $\phi(T_c)/T_c$ is [22]

$$\frac{\phi(T_c)}{T_c} \approx \frac{2}{\lambda_\phi} \left(\frac{m_V^3}{3\pi v_\phi^3} \right) = \frac{2g_X^3}{3\pi\lambda_\phi} \quad (4.26)$$

Hence, for g_X satisfying Eq. (4.4) with $m_V \lesssim \mathcal{O}(1)$ TeV and $m_\phi \gtrsim \mathcal{O}(10)$ GeV, the phase transition is nearly of the second-order type (i.e. $\phi(T_c)/T_c \ll 1$). In this case, based on the Kibble-Zurek mechanism [23, 24], the initial abundance of monopole at its formation is expected to be [25]

$$Y_i \approx \frac{(\sqrt{\lambda_\phi/2})^3}{C_S} \left[\frac{1}{\sqrt{\lambda_\phi/2}} C_0^{1/2} \frac{m_M}{g_M M_{\text{P}}} \right]^{3\nu/(1+\mu)} \quad (4.27)$$

where $Y_i \equiv n_i/s$ with n_i and s being respectively the number density of monopoles and entropy density, $C_S \equiv \left(\frac{2\pi^2}{45} g_{*S} \right)$, $C_0 \equiv \left(\frac{\pi^2}{90} g_* \right)$ with g_{*S} and g_* being respectively the relativistic degrees of freedom associated with entropy and energy densities, and $g_M \equiv 4\pi/g_X$ is the magnetic charge of monopoles. For a negligible Hubble expansion rate, the classical values of the critical exponents are $\nu = \mu = 1/2$, but quantum corrections increase them to $\nu = \mu = 0.7$ [25].

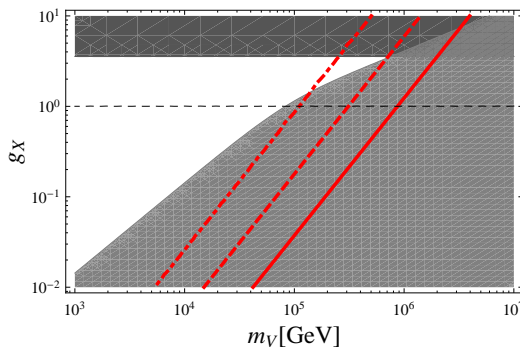


Figure 8. Contours of the relic abundance of monopoles, corresponding to $\Omega_M/\Omega_{\text{CDM}} = 10^{-2}, 0.1, 1$ for dot-dashed, dashed and solid lines, respectively. Gray and dark-gray regions are excluded due to too much VDM and perturbativity of gauge coupling, respectively. Eq. (4.23) was used for the VDM relic density with $m_\phi = 2m_V$ and $\Delta m_V/m_V = 10^{-4}$.

The initial abundance of monopoles may be reduced further by monopole-antimonopole annihilation resulting from formation of a magnetic Coulomb bound state and its subsequent cascade decays into dark photons [26]. However in our scenario the annihilation caused by such collisions are not efficient enough to reduce monopole density further than that in Eq. (4.27). This is because in the thermal bath only V^\pm which have dark charge interact directly with monopoles. In order to reduce monopole density significantly, V^\pm should be light enough. This means that for a given v_ϕ , g_X should be small enough, but this results in very heavy monopoles and the effect of g_X to the fractional energy density of monopoles is cancelled out. In addition, v_ϕ is subject to the constraint Eq. (4.4), and g_X should not be too small to avoid over-production of dark matter. Hence, v_ϕ can not be small and, as the result, the energy contribution of monopole can not be reduced much. One may expect that the mixing between dark and visible sector Higgses may results in a sizable reduction of monopole density due to the interactions to SM particles. However note that the mixing angle α is constrained to be less than about 0.45 for 95% CL [11]. So, its effect is at most comparable to the case of V^\pm for $m_V \lesssim \mathcal{O}(1)$ TeV.

Fig. 8 shows contours of thermal relic density of hidden sector monopoles as a function of g_X and m_V , which was obtained from Eq. (4.27). We notice that the monopole abundance can be about 10% of the observed dark matter relic density at best in the price of $10^{-2}\%$ tuning of m_V at $\mathcal{O}(1)$ PeV scale, even though we take $\alpha_X \sim \mathcal{O}(1)$ for which perturbative description of our model may be not valid any more. Hence VDM should be the main component of the present dark matter relic density, and in this case the mass of VDM is constrained to be close to or smaller than $m_h/2$ as discussed in the previous subsections. The relic abundance of monopoles turns out to be $\Omega_M \sim \mathcal{O}(10^{-6} - 10^{-5})\Omega_{\text{CDM}}$ for such a light VDM, which is totally negligible. Still the existence of hidden sector monopole is very crucial to guarantee the hidden sector VDM V_μ^\pm to be absolutely stable due to the unbroken $U(1)_X$ subgroup of the original $SU(2)_X$.

4.4 Direct Detection

4.4.1 VDMs

As in the Abelian VDM case, the direct detection cross section of VDM-nucleon scattering occurs through the t -channel exchange of H_1 and H_2 . Due to the generic destructive inter-

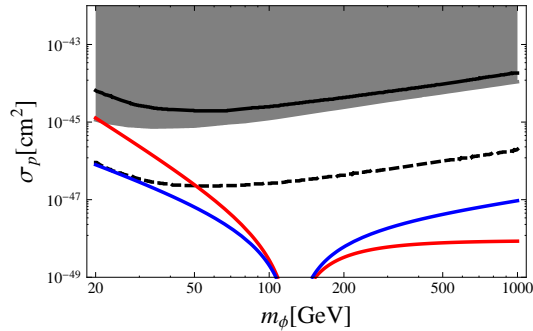


Figure 9. Spin-independent direct detection cross section of VDM (red and blue lines) at each resonance as a function of m_ϕ in the small mixing limit ($\alpha = 0.1$) with $\alpha_X = \alpha_X^{\max}$. Red lines: $m_V \approx m_h/2$ and we chose $\lambda_H = 0.140$ for the vacuum stability of SM Higgs potential. Blue lines: $m_V \approx m_\phi/2$. Light gray region is excluded by LUX experiment. The solid and the dashed black line is the XENON100 bound and the projected bound of XENON1T experiment. Regions below red and blue lines in each case of resonance are consistent with Eq. (4.4).

ference between two scalar bosons, the strong bounds from the CDMS and XENON100 can be significantly relaxed if $m_1 \sim m_2$, as shown in Ref. [8].

The spin-independent elastic cross section σ_p of the VDM V^\pm scattering off the proton is obtained as [8]

$$\sigma_p = \frac{4\mu_V^2}{\pi} \left(\frac{g_X s_\alpha c_\alpha m_p}{2v_H} \right)^2 \left(\frac{1}{m_1^2} - \frac{1}{m_2^2} \right)^2 f_p^2, \quad (4.28)$$

where $\mu_V = m_V m_p / (m_V + m_p)$, m_p being the proton mass, and $f_p = \sum_{q=u,d,s} f_q^p + 2/9(1 - \sum_{q=u,d,s} f_q^p) \approx 0.468$ [28]. As an example, Fig. 9 depicts the spin-independent direct detection cross section σ_p for each resonance with $\alpha = 0.1$ (which can be valid up to $m_2 \simeq 1$ TeV) and g_X saturating the bound in Eq. (4.4). As shown in the figure, all region of $m_\phi \gtrsim 20$ GeV can satisfy XENON100 and LUX bounds [29] which is the most strong constraint as of now. In addition, XENON1T [30] may probe $m_\phi \lesssim 50$ GeV for $\sqrt{s} \approx m_h$ in optimistic cases.

4.4.2 Monopoles

The monopole in our scenario is neutral under SM gauge group, and it interacts with the SM particles only via Higgs mediation thanks to the Higgs portal interaction we newly introduced in this paper. The interaction is similar to that of DM-nucleon scattering via Higgs mediation. However monopoles may be regarded as a particle located at the classical field ϕ_c (the solution for the classical field equation describing a monopole configuration) vanishes. Then, the monopole-nucleon scattering cross section may be given by

$$\frac{d\sigma_p}{d\Omega} = \frac{\mu_M^2}{4\pi^2} \left[\frac{\lambda_{\Phi H}}{8} \frac{m_p}{m_M} \left| \frac{f_p}{t - m_h^2} \right| \right]^2 \quad (4.29)$$

where $\mu_M = m_M m_p / (m_M + m_p)$ with t is the Mandelstam variable. Note that, for the recoil energy E_r of target atom in a direct search experiment, $t = -2m_A E_r$ with m_A being the mass

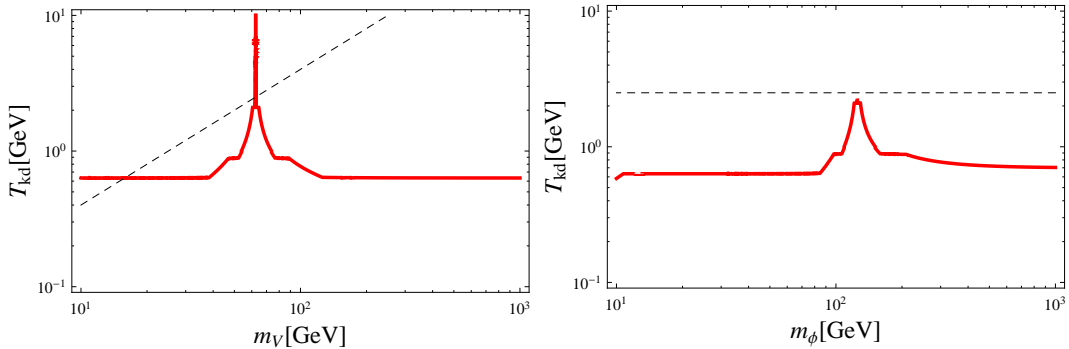


Figure 10. Temperatures of photon at the kinetic decoupling of dark matter from SM thermal bath for $\alpha = 0.1$. Left: $\sqrt{s} = m_\phi$. Right: $\sqrt{s} = m_h$. We used $\alpha_X = \alpha_X^{\max}/\sqrt{10}$. Dashed lines are $T_{fz} = m_V/25$ for each resonance.

of target atom. Hence, for $E_r \lesssim m_h^2/(2m_A)$, we find

$$\begin{aligned} \sigma_p &\lesssim \frac{\lambda_{\Phi H}^2}{64\pi m_M^2} \left(\frac{m_p}{m_h}\right)^4 f_p^2 \\ &\simeq \frac{3.4 \times 10^{-28}}{\text{GeV}^2} \left(\frac{\lambda_{\Phi H}}{0.1}\right)^2 \left(\frac{10^7 \text{ GeV}}{m_M}\right)^2 \end{aligned} \quad (4.30)$$

It is far below sensitivities of present or near-future direct search experiments.

5 Dark Radiation

The massless dark photon associated with the unbroken dark $U(1)_X$ symmetry contributes to the extra relativistic degrees of freedom in the present universe. Starting from thermal equilibrium at high temperature, it is decoupled from VDM at $T_\gamma \sim 10$ MeV for a maximally allowed g_X in Eq. (4.4) [14]. However, VDM is decoupled from SM thermal bath at much higher temperature since the thermal equilibrium of VDM is maintained only by Higgs mediation.

For a relativistic particle in thermal bath, the thermal-averaged scattering cross section of dark matter to a SM fermion is found to be

$$\langle\sigma v\rangle_f \simeq 2\alpha_X s_\alpha^2 c_\alpha^2 \left| \frac{1}{m_1^2} - \frac{1}{m_2^2} \right|^2 \frac{m_f^2}{v_H^2} E_f^2 \quad (5.1)$$

where we assumed that the momentum transfer is negligible relative to m_1 and E_f is the energy of the SM fermion. The scattering rate of DM to SM particles is then given by

$$\Gamma_s = \sum_f n_f \langle\sigma v\rangle_f \quad (5.2)$$

where f represents a SM fermion, and n_f is its number density. The kinetic decoupling takes place as the scattering rate of DM to SM particles becomes smaller than the Hubble expansion rate. Let us take the scalar mixing angle α to be $\alpha = 0.1$ for simplicity. Then, as shown in Fig. 10, $T_{\text{QCD}} < T_{\text{kd}} < 1$ GeV for most of region. Even for $m_1 \sim m_2$, we

find $T_{\text{kd}} < T_{\text{fz}} \sim 2 \text{ GeV}$ except the case of very high degeneracy. Note that $T_{\text{kd}} > T_{\text{fz}}$ for $m_V \sim 10 \text{ GeV}$. In this case, VDM is in chemical equilibrium even after kinetic decoupling. Since, as shown in Section 4.2, VDM interacts strongly enough with dark photon to keep kinetic equilibrium, its kinetic energy at its production from SM thermal bath is redistributed among VDM and dark photons. However, the kinetic energy is negligible relative to the energy of dark photon, hence temperature of dark photon is not changed. Therefore, we can say that the kinetic decoupling temperature is $T_{\text{QCD}} < T_{\text{kd}} \lesssim \mathcal{O}(1) \text{ GeV}$, and the contribution of dark photon to the present radiation energy density as the extra neutrino species can be $\Delta N_{\text{eff}}^\nu \simeq 0.08 - 0.11$. It is consistent with the recent result of Planck satellite mission [1], and can be probed at a Stage-IV CMB experiment at 2σ -level [31]. Note that we could make a definite prediction to the amount of dark radiation from massless dark photon, based on an unbroken local dark gauge symmetry and thermal VDM with a Higgs portal interaction. This is in sharp contrast to other models for extra dark radiations from, for example, axions or sterile neutrinos whose energy densities are usually adjusted by hand to match observations.

6 Conclusions

In this paper, as a logically natural extension of SM to a dark sector in regard of local gauge principle and the stability of dark matter, we considered a $SU(2)$ dark gauge symmetry which is broken to $U(1)_X$ by a $SU(2)$ -triplet dark Higgs field, which is the t'Hooft-Polyakov monopole model in the dark sector with Higgs portal. In this model, the dark sector consists of monopoles and massive vector bosons, both of which are stable due to topology and unbroken $U(1)_X$ respectively, and massless dark photons. Although the constraint from CMB data on the dark matter annihilation cross section is quite stringent, we showed that a right amount of thermal relic density can be obtained by resonant thermal freeze-out of massive VDM when the mass of VDM is close to or smaller than one for SM Higgs resonance, thanks to the Higgs portal which was newly introduced in this work.

The abundance of monopoles turns out to be negligible in this case, and their role as CDM is not very important. However their existence is crucial for the VDM to be absolutely stable in the presence of higher dimensional nonrenormalizable operators, due to the unbroken $U(1)_X$. Present direct searches do not constrain VDM mass of $\mathcal{O}(10 - 10^3) \text{ GeV}$. But XENON1T experiment for example may probe VDM mass less than about 60 GeV . The massless dark photon associated with the $U(1)_X$ contributes to the present radiation energy density, resulting in $\Delta N_{\text{eff}}^\nu \sim 0.1$ as the extra relativistic neutrino species.

Our hidden monopoles are quite rare and their scattering rate to nucleons looks too small to be detected at direct search experiments. However, the self-interaction of monopoles, characterized by $g_M \equiv 4\pi/g_X$ is quite large for a small g_X , and it may cause monopoles captured at astrophysical object like sun. In this case, the captured monopoles may be able to annihilate, and leave observable imprints. We will take a look at this possibility in other place.

Acknowledgments

We are grateful to Yuji Omura for collaboration at the initial stage, and to B. Holdom, Kimyeong Lee and E. Weinberg for useful discussion. This work was supported by NRF Research Grant 2012R1A2A1A01006053, and by SRC program of NRF Grant No. 20120001176 funded by MEST through Korea Neutrino Research Center at Seoul National University.

References

- [1] P. A. R. Ade *et al.* [Planck Collaboration], arXiv:1303.5076 [astro-ph.CO].
- [2] S. Baek, P. Ko and W. -I. Park, JHEP **1307**, 013 (2013)
- [3] G. Shiu, P. Soler and F. Ye, Phys. Rev. Lett. **110**, 241304 (2013)
- [4] G. 't Hooft, Nucl. Phys. B **79**, 276 (1974).
- [5] A. M. Polyakov, JETP Lett. **20**, 194 (1974) [Pisma Zh. Eksp. Teor. Fiz. **20**, 430 (1974)].
- [6] S. Baek, P. Ko and W. -I. Park, JHEP **1202**, 047 (2012)
- [7] S. Baek, P. Ko, W. -I. Park and E. Senaha, JHEP **1211**, 116 (2012)
- [8] S. Baek, P. Ko, W. -I. Park and E. Senaha, JHEP **1305**, 036 (2013)
- [9] T. Hambye, JHEP **0901**, 028 (2009)
- [10] R. Barate *et al.* [LEP Working Group for Higgs boson searches and ALEPH and DELPHI and L3 and OPAL Collaborations], Phys. Lett. B **565**, 61 (2003) [hep-ex/0306033].
- [11] S. Choi, S. Jung and P. Ko, JHEP **1310**, 225 (2013) [arXiv:1307.3948].
- [12] A. Sommerfeld, Annalen der Physik **403**, 257 (1931).
- [13] N. Arkani-Hamed, D. P. Finkbeiner, T. R. Slatyer and N. Weiner, Phys. Rev. D **79**, 015014 (2009) [arXiv:0810.0713 [hep-ph]].
- [14] J. L. Feng, M. Kaplinghat, H. Tu and H. -B. Yu, JCAP **0907**, 004 (2009)
- [15] J. P. Ostriker, Phys. Rev. Lett. **84**, 5258 (2000) [astro-ph/9912548].
- [16] A. Loeb and N. Weiner, Phys. Rev. Lett. **106**, 171302 (2011) [arXiv:1011.6374 [astro-ph.CO]].
- [17] M. Vogelsberger, J. Zavala and A. Loeb, Mon. Not. Roy. Astron. Soc. **423**, 3740 (2012)
- [18] M. S. Madhavacheril, N. Sehgal and T. R. Slatyer, arXiv:1310.3815 [astro-ph.CO].
- [19] K. -J. Ahn and P. R. Shapiro, Mon. Not. Roy. Astron. Soc. **363**, 1092 (2005) [astro-ph/0412169].
- [20] F. -Y. Cyr-Racine, R. de Putter, A. Raccanelli and K. Sigurdson, arXiv:1310.3278 [astro-ph.CO].
- [21] A. R. Zentner, Phys. Rev. D **80**, 063501 (2009) [arXiv:0907.3448 [astro-ph.HE]].
- [22] M. Dine, R. G. Leigh, P. Huet, A. D. Linde and D. A. Linde, Phys. Lett. B **283**, 319 (1992)
- [23] T. W. B. Kibble, J. Phys. A **9**, 1387 (1976).
- [24] W. H. Zurek, Nature **317**, 505 (1985).
- [25] H. Murayama and J. Shu, Phys. Lett. B **686**, 162 (2010)
- [26] J. Preskill, Phys. Rev. Lett. **43**, 1365 (1979).
- [27] P. Gondolo and G. Gelmini, Nucl. Phys. B **360**, 145 (1991).
- [28] G. Belanger, F. Boudjema, A. Pukhov and A. Semenov, Comput. Phys. Commun. **180**, 747 (2009)
- [29] D. S. Akerib *et al.* [LUX Collaboration], arXiv:1310.8214 [astro-ph.CO].
- [30] E. Aprile [XENON1T Collaboration], arXiv:1206.6288 [astro-ph.IM].
- [31] K. N. Abazajian, K. Arnold, J. Austermann, B. A. Benson, C. Bischoff, J. Bock, J. R. Bond and J. Borrill *et al.*, arXiv:1309.5383 [astro-ph.CO].